Interplay between charge, orbital, and magnetic ordering in $La_{1-x}Sr_xMnO_3$

G.-L. Liu, J.-S. Zhou, and J. B. Goodenough
Texas Materials Institute, ETC 9.102, University of Texas at Austin, Austin, Texas 78712-1063
(Received 2 April 2001; published 19 September 2001)

The evolution with x of the complex phase diagram below 310 K of $La_{1-x}Sr_xMnO_3$ in the range $0 \leqslant x \leqslant 0.35$ has been mapped out with measurements on a series of melt-grown samples of resistivity $\rho(T)$, specific heat $C_p(T)$, magnetization $M(T)$ in applied magnetic fields $H=20$ Oe, 5 kOe, and magnetization at 5 K up to 50 kOe. Between the canted-spin antiferromagnetic insulator and ferromagnetic metal (FM) phases, an unusual interplay between charge, orbital, and magnetic ordering is revealed. In the paramagnetic range $T_c<T<T_{JT}$ the electrons of *e*-orbital parentage are preferentially ordered into (001) planes and the system exhibits a colossal magnetoresistance. At temperatures below a $T_{oo}<T_c$, a different orbital order is found; in an applied magnetic field it is associated with a ferromagnetic insulator (FI) phase. In a narrow temperature interval $T_{oo}<T<T_c$, the system is conductive and a spin glass in an applied magnetic field $H=20$ Oe is transformed by $H=5$ kOe into a ferromagnetic vibronic phase. As the cooperative orbital-ordering temperature T_{JT} decreases with increasing x, the transition at T_{JT} changes from second-order to first-order. In $H=50$ kOe at 5 K, the magnetization of the FI phase exceeds the theoretical spin-only value of $(4-x)\mu_B$/Mn, reaching 4.4 μ_B/Mn at $x=0.15$; the magnetization of the FM phase has the spin-only value.

DOI: 10.1103/PhysRevB.64.144414 PACS number(s): 75.40.−s, 75.50.Lk, 71.70.Ej

INTRODUCTION

The $Ln_{1-x}A_xMnO_3$ (Ln=lanthanide, A=alkaline-earth) perovskites have been studied intensively in recent years because they exhibit such unusual properties as a colossal magnetoresistance (CMR) and spin-glass behavior. These unusual properties are found at a crossover from antiferromagnetic to ferromagnetic order where the σ-bonding $3d$ electrons change from a localized to an itinerant character while the π-bonding $3d$ electrons remain localized with a spin $S=\frac{3}{2}$ on every Mn atom. In addition, the σ-bonding electrons have an orbital degeneracy that results in cooperative Jahn-Teller orbital ordering where the σ-bonding electrons are localized. The interplay between spin, charge, and orbital degrees of freedom has provided an important challenge to existing theories of electronic states in solids. In this paper we report a systematic series of measurements, including specific heat, on melt-grown crystals of $La_{1-x}Sr_xMnO_3$ across the compositional range $0 \leqslant x \leqslant 0.35$ with special emphasis on the range $0.08 \leqslant x \leqslant 0.19$ where the phase diagram has been shown to be particularly complex; a crossover from canted-spin antiferromagnetic insulator to ferromagnetic metal occurs with increasing x in this compositional range.

$LaMnO_3$ contains a localized $t^3e^1 3d$-electron configuration at the octahedral-site Mn(III) ions. The *e*-orbital degeneracy is removed by locally cooperative oxygen displacements that fluctuate in three dimensions (3D) at temperatures $T>T_{JT}$ and in 2D within (001) planes in the interval $T^*<T<T_{JT}$ ($T^* \approx 600$ K, $T_{JT} \approx 750$ K); on cooling below T^*, the cooperative oxygen displacements are static.[1] The 3D bond-length fluctuations above T_{JT} allow breathing-mode oxygen displacements that give rise to a disproportionation charge transfer 2Mn(III)=Mn(II)+Mn(IV) on a fraction of the Mn sites. Therefore, there is a transition from an insulator to a conductive phase at T_{JT}. Moreover, ordering of the occupied *e* orbitals into the (001) planes below T_{JT} confines the dominant ferromagnetic σ-bond superexchange interactions to the (001) planes; the π-bond superexchange interactions dominate along the [001] axis to give an antiferromagnetic coupling between the ferromagnetic (001) planes.[2] A Dzialoslinskii antisymmetric superexchange term cants the antiferromagnetic spins to give a weak ferromagnetic component below the Néel temperature $T_N=145$ K; the canted-spin antiferromagnetic (CAF) order is classified as A_yF_z in space group Pbnm.[3]

The system $La_{1-x}Sr_xMnO_3$ retains localized t^3 configurations with spin $S=\frac{3}{2}$ on all the Mn atoms; in the compositional range $0.08 \leqslant x \leqslant 0.18$, the x holes/Mn atom in the σ-bonding states of *e*-orbital parentage undergo a transition from polaronic behavior in the canted-spin antiferromagnetic insulator phase (CAFI) to itinerant behavior in a ferromagnetic metallic (FM) phase. A combination of (1) transport measurements [thermoelectric power $\alpha(T)$ and resistivity $\rho(T)$] under hydrostatic pressure on selected single crystals,[4] (2) structural studies with neutron diffraction,[5] and (3) magnetic data[6] in and across this compositional range have revealed that the transition from polaronic to itinerant behavior of the holes of *e*-orbital parentage proceeds by a series of distinguishable phases, which gives rise to a complex phase diagram. We report here transport, magnetic, and specific-heat measurements on a series of melt-grown crystals that confirm the complex evolution of phases in the range $0.08 \leqslant x \leqslant 0.19$ and establish the atmospheric-pressure phase boundaries shown in Fig. 1. Extrapolation between the experimental points in Fig. 1 is based on the pressure studies[4] that have shown discontinuous jumps in T_c where it crosses T_{JT}, a vibronic-to-metallic transition at $x \approx 0.15$, and the orthorhombic-rhombohedral transition at T_{OR}. The first-order insulator-metal transition at T_{IM} was found[4] to descend with increasing x to about 130 K where it ended in a phase segregation.

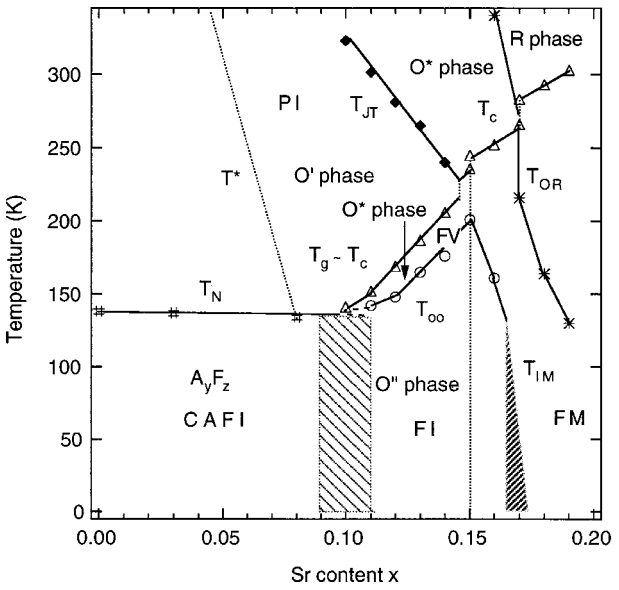

FIG. 1. Phase diagram for $La_{1-x}Sr_xMnO_3$, $0 \leqslant x \leqslant 0.20$. Experimental points above 310 K taken from the literature; T_N and two values of T_c for $x=0.17$ taken from $M(T)$; two values of T_c for $x=0.15$ taken from $C_p(T)$; all other points taken from Fig. 2.

A colossal magnetoresistance (CMR) found[7] above T_c in the compositional range $0.10 \leqslant x \leqslant 0.15$ has been modeled as a dynamic phase segregation within a paramagnetic matrix of a ferromagnetic metal (FM) phase having a T_c higher than an antiferromagnetic ordering temperature T_N of the matrix. In this model, the ferromagnetic conductive phase of higher T_c grows above T_N of the matrix in an applied magnetic field H to beyond a percolation threshold.[8] This model calls for an antiferromagnetic ordering of the matrix below T_N as in the CAFI phase and therefore a spin-glass behavior below a T_g if the orbital ordering of the matrix remains that of the O structure.

We have measured the specific heat and magnetization in an applied field $H=20$ kOe in order to determine whether the spin system orders as a spin glass below a $T_g \approx T_c$ in low applied magnetic fields H and is globally transformed to ferromagnetic order in higher H fields. The specific-heat data have also allowed investigation of the prediction[9] that the localized-to-itinerant electronic transition would change from second-order to first-order as it decreases towards T_c and verification of the first-order character of the orbital-ordering transition at T_{oo} in a narrow compositional range about $x=0.115$.

EXPERIMENTAL PROCEDURES

Crystals of $La_{1-x}Sr_xMnO_3 (0 \leqslant x \leqslant 0.19)$ were grown by the floating-zone method in an IR-radiation image furnace. The polycrystalline feed rods were prepared from a stoichiometric mixture of La_2O_3, $SrCO_3$, and Mn_2O_3 that had been calcined three times at 1050 °C with interanneal grinding. The resulting powder was pressed into a rod and sintered at 1350 °C for 24 h. Crystals with $0 < x \leqslant 0.1$ were grown in Ar; those with $x > 0.1$ were grown in flowing air. This process has been shown to yield oxygen-stoichiometric crystals close to the nominal composition.[6,10] The melt-grown rods tend to contain numerous large crystals, but independent measurements on single-crystal specimens showed no difference in the temperature dependence of the resistivity in different crystallographic directions, only a small difference in magnitude. Of interest in this study is the temperature dependence of the resistivity; it was obtained on cooling and warming by four-probe measurements made on bars cut from the melt-grown samples. The critical temperatures are more sharply defined in the melt-grown samples than in polycrystalline samples.

The specific heat $C_p(T)$ was measured with the relaxation method.[11] The instrument was calibrated by measuring $C_p(T)$ for sapphire and a high-quality single crystal of Fe_3O_4. The dc magnetization was obtained with a SQUID (Quantum Design) magnetometer.

RESULTS AND DISCUSSION

Figure 2 shows the temperature dependence of the resistivity $\rho(T)$ of the melt-grown samples. The data are consistent with those reported in the literature[4,6,12] for melt-grown samples, but they represent finer steps in x over the entire range $0.08 \leqslant x \leqslant 0.19$. Data taken on polycrystalline samples in this range[5] show no major discrepancies from those taken on melt-grown samples. The critical temperatures marked on these curves were obtained as described in the caption of Fig. 2. The transition from insulator to metallic conduction at low temperature in the interval $0.15 < x < 0.18$ shows that the holes are more mobile below T_{IM} than below T_{oo} and that the metallic phase dominates the $\rho(T)$ data in the $x=0.17$ sample, which is shown below to be two phase.

The magnetization data of Fig. 3 were obtained at 5 K in a magnetic field $H=50$ kOe. The inset of Fig. 3 shows typical $M(H)$ curves. The straight line in the main figure corresponds to the theoretical spin-only value $(4-x)\mu_B$/Mn of the magnetization for collinear-spin ferromagnetism. The rapid rise of $M(5\text{ K},50\text{ kOe})$ from that of a weak canted-spin ferromagnet below an antiferromagnetic Néel temperature T_N to collinear-spin ferromagnetism in a modest applied field H in the interval $0.08 \leqslant x \leqslant 0.11$ represents the coexistence of ferromagnetic and antiferromagnetic regions as will become clear below; the rise in $M(5\text{ K},50\text{ kOe})$ does not represent a continuous increase in the cant angle as was predicted by de Gennes[13] on the basis of a homogeneous magnetic system with itinerant e electrons in a narrow σ^* band. In the range $x \geqslant 0.18$ where the system is a ferromagnetic metal, the saturation magnetization at 5 K and 50 kOe has the theoretical spin-only value $M_S=(4-x)\mu_B$/Mn. However, an $M(5\text{ K},50\text{ kOe}) > (4-x)\mu_B$/Mn is observed in the intermediate range $0.11 < x < 0.18$ of the orbitally ordered O'' phase, reaching a maximum value of $4.4\,\mu_B$/Mn at $x=0.15$. A high magnetic moment ($4.2\,\mu_B$/Mn) for $x=0.15$ has also been reported without comment by others.[6] This enhancement of the saturation magnetization is unique to the O'' phase of the $La_{1-x}Sr_xMnO_3$ system; it has not been observed in the

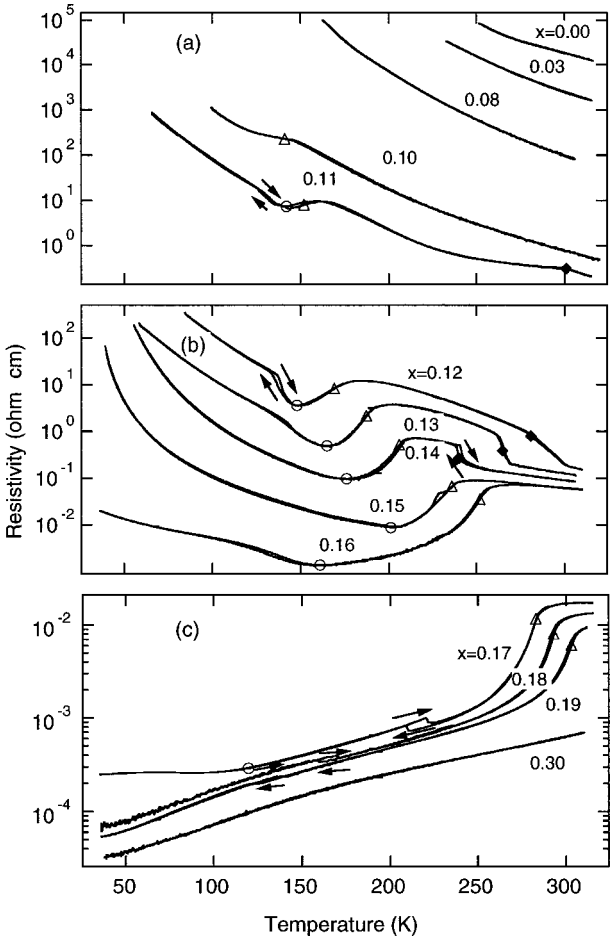

FIG. 2. Resistivity versus temperature for melt-grown samples of $La_{1-x}Sr_xMnO_3$. Critical points: $\blacklozenge = T_{JT}$ where $|d\rho/dT|$ is a maximum; $\Delta = T_g \approx T_c$ where $d\rho/dT$ is a maximum; $\bigcirc = T_{oo}$ where $\rho(T)$ is a local minimum; T_{OR} = midpoint of thermal hysteresis below T_c for $0.17 \leqslant x \leqslant 0.19$. Arrows indicate heating and cooling at thermal hysteresis loops.

$La_{1-x}Ca_xMnO_3$ system where the insulator O'' phase does not occur. Although the orbital angular momentum is quenched in lowest-order perturbation theory at both Mn(III) and Mn(IV) in octahedral sites, the data indicate that where the Mn(III) e electrons are localized, an orbital contribution to the atomic moment is introduced by higher-order terms; where the electrons of e-orbital parentage are itinerant, the orbital contribution is suppressed. The orbital contribution appears to be progressively suppressed as the hole mobility in the O'' phase increases with x in the range $0.15 < x < 0.18$.

Figure 4 compares the specific heat $C_p(T)$ with the magnetization $M(T)$ obtained in fields $H = 20$ Oe and 5 kOe either on heating after cooling in zero field (ZFC) or on cooling in the measuring field (FC). A correction for the remanent field in the SQUID magnetometer was made to obtain $M(T)$ in a field as low as $H = 20$ Oe. The several critical temperatures of Fig. 1 are also marked by arrows in these figures; they correspond well with transitions indicated in the $C_p(T)$ and $M(T)$ data.

For sample $x = 0.0$ and 0.03 of Fig. 4, a $T^* > 300$ K is not

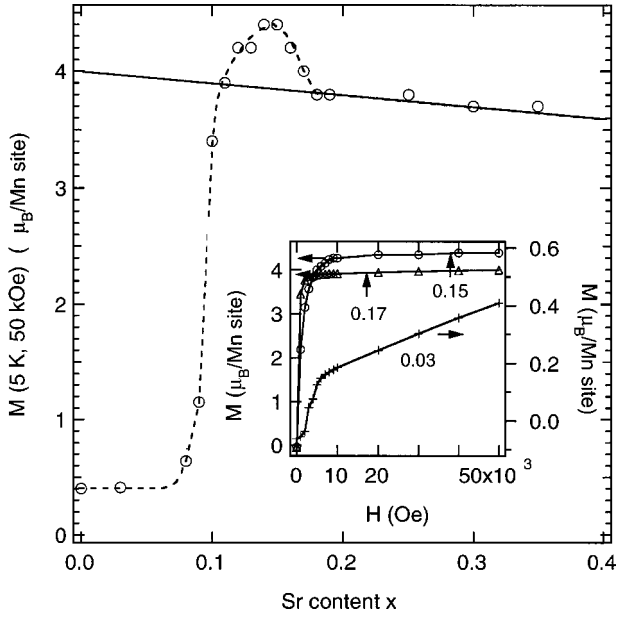

FIG. 3. Magnetization at 5 K in 50 kOe for $La_{1-x}Sr_xMnO_3$, $0 \leqslant x \leqslant 0.35$. Solid line: $(4-x)\mu_B$/Mn. Inset: $M(5\text{ K})$ versus applied field. Dashed line is a guide to the eye.

crossed as measurements were made for $T < 310$ K; the $x = 0.08$ sample appears to have a $T^* \approx T_N$. Therefore, the only critical temperature appearing in Figs. 4(a)–4(c) is T_N. The $C_p(T)$ data for the $x = 0.0$ and 0.03 samples show a typical second-order anomaly at T_N, and the magnetization may be understood with a canted-spin antiferromagnetic model. However, $C_p(T)$ for the $x = 0.08$ sample has a suppressed entropy change at T_N and an anomaly characteristic of a higher-order transition. Considerable short-range magnetic order far above T_N and/or a freezing of the spins at T_N without much change in the long-range order is evident.

The $C_p(T)$ data of Fig. 4(d) show a suppressed entropy change at the transition temperature $T_c \geqslant T_{oo}$ in the $x = 0.10$ sample, and the $M(T)$ data in $H = 20$ Oe are typical of a spin glass. The enhancement of $M(T)$ below 100 K in the FC data indicates the coexistence of the CAFI phase having $T_N \approx 135$ K. In $H = 5$ kOe, the spin-glass phase is transformed into a ferromagnetic phase with a Curie temperature $T_c \approx T_g$, but the CAFI phase remains unchanged to give an enhancement of $M(T)$ below 100 K. The coexistence of the CAFI phase keeps $M(5\text{ K}, 50\text{ kOe})$, Fig. 3, below the theoretical spin-only value. The data thus provide clear evidence of the coexistence of two magnetic phases, one corresponding to the CAFI phase and the other to a peculiar phase that is a spin glass in low magnetic fields and is transformed into a ferromagnetic phase in an applied filed $H = 5$ kOe. Evidence for the CAFI phase does not appear in the $H = 20$ Oe $M(T)$ data of Fig. 4(e) for $x = 0.11$, but a spin glass appears below $T_g \approx T_c$ as in the $x = 0.10$ sample; the transition at $T_{00} < T_c$ is clearly first order.

A spin glass would occur where an antiferromagnetic matrix ordering below its $T_N = T_g$ contains within it a volume of FM phase that is below its percolation limit and has a $T_c(\text{FM}) > T_g$. In the manganese-oxide perovskites, the FM

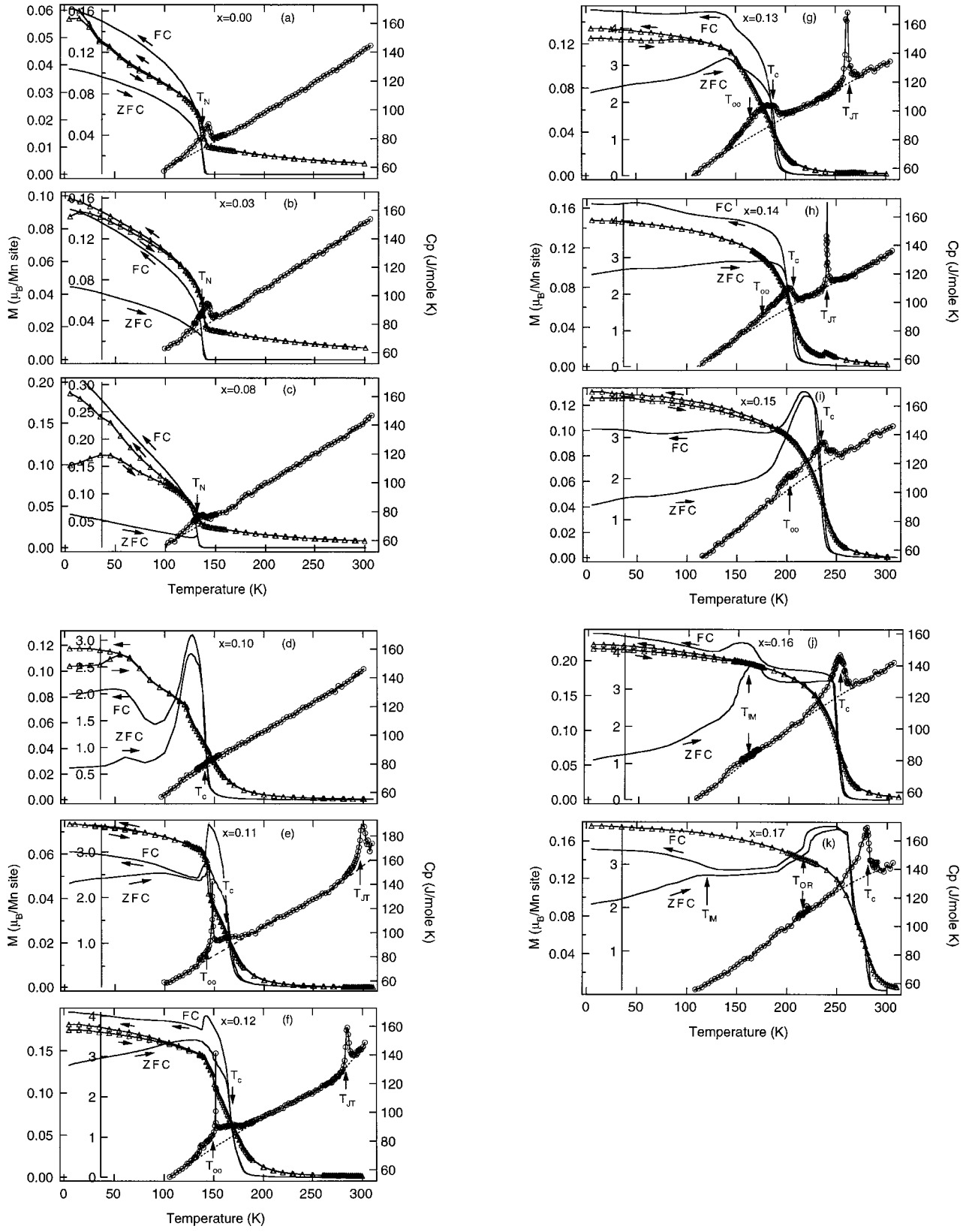

FIG. 4. Magnetization $M(T)$ in $H=20$ Oe and 5 kOe; specific heat $C_p(T)$ for $La_{1-x}Sr_xMnO_3$. $\bigcirc = C_p$; $\Delta = M(T)$ in 5 kOe; simple solid line $= M(T)$ in 20 Oe. Arrows indicate warming vs cooling curves.

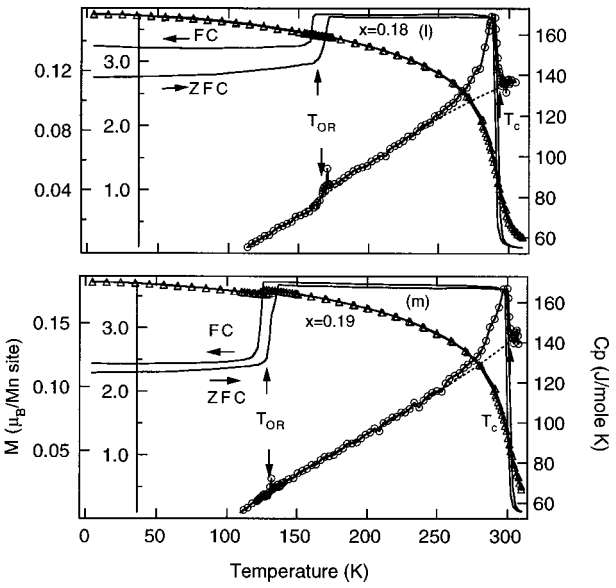

FIG. 4. (*Continued*).

phase is hole-rich, the matrix is hole poor.[8] The concentration of holes within a FM volume exceeds $x=0.15$. Interpretation of the magnetic and transport data requires a distinction be made between what happens when a field H is applied above T_g where the samples are paramagnetic and the phase transition that occurs on application of a modest $H=5$ kOe below T_g. At paramagnetic temperatures $T_g<T<T_c$(FM), the FM phase grows to beyond its percolation threshold in a large H, and the CMR phenomenon reflects the greater conductivity of the FM phase. The application of an H below T_g, on the other hand, induces a global transformation of the antiferromagnetic matrix of the spin glass to a ferromagnetic phase in which the holes trapped in the FM clusters become released as two-manganese Zener polarons.[4]

We can understand such a global magnetic phase transition if we recognize that 3D ferromagnetic Mn(III)-O-Mn(III) superexchange interactions occur where the cooperative, local Jahn-Teller deformations fluctuate;[14] static Jahn-Teller deformations give rise to antiferromagnetic t^3-O-t^3 superexchange interactions in at least one direction, as occurs in the O' phase along the c-axis. Stabilization of 3D relative to 2D ferromagnetic interactions in an applied magnetic field H would involve transforming 2D orbital fluctuations in an O' matrix in the range $T^*<T<T_{\rm JT}$ into 3D orbital fluctuations in an O^* matrix. Evidence that an applied H stabilizes an O^* relative to an O' matrix in the interval $T^*<T<T_{\rm JT}$ even in the paramagnetic phase is found in a report by Uhlenbruck *et al.*[15] that $T_{\rm JT}$ is lowered and T_c is raised in an $H=140$ kOe in an $x=0.125$ sample. Our data show similar, but smaller, shifts of $T_{\rm JT}$ and T_c in an $H=50$ kOe.

The O^*-O' transition at T_c is unusual in another respect since the higher-temperature phase has the greater orbital order along with a greater magnetic disorder. In a magnetic field, magnetic ordering below T_c is accompanied by long-range orbital disorder in the narrow temperature interval $T_{oo}<T<T_c$; in this interval, there is a transition to a different long-range orbital ordering below T_{oo}. Therefore, it should not be surprising that the application of an H below T_c is able to disrupt the long-range orbital ordering with 2D orbital fluctuations that occurs in the O' phase above T_c.

In the compositional range $0.11\leqslant x\leqslant 0.14$, a $T_c<T_{\rm JT}<310$ K gives a conspicuous anomaly in $C_p(T)$ at $T_{\rm JT}$. The data of Figs. 4(e)–4(h) show a clear evolution from a second-order to a first-order transition as $T_{\rm JT}$ is lowered. Rozenberg *et al.* [9] have predicted a similar change should occur at a transition from localized to itinerant electronic behavior; the e electrons are localized or confined to two-manganese polarons for $T<T_{\rm JT}$, but they approach an itinerant character at $T>T_{\rm JT}$ as x approaches $x=0.15$; for $x>0.15$, a first-order insulator-metal transition occurs at T_{IM}.

In agreement with the conductivity data of Fig. 2, $C_p(T)$ shows that the transition at T_{oo} is first-order in the $x=0.11$ and $x=0.12$ samples, but is similar to a glass transition in the other compositions. Apparently long-range order of the occupied e orbitals sets in at T_{oo} in only a narrow range of compositions $0.11\leqslant x\leqslant 0.12$; in the O'' compositions away from this range, the orbital ordering that occurs on cooling through T_{oo} consists of considerable short-range order in the spin-glass or FV phase and retains short-range fluctuations well below the long-range orbital-ordering temperature T_{oo}.

Figures 4(f), 4(g) show a peculiar enhancement of $M(T)$ in a finite temperature interval below T_{oo} in a field $H=20$ Oe. From the $C_p(T)$ data, the enhancement occurs where the entropy is changing sharply with temperature on crossing an order-disorder transition. A similar enhancement of $M(T)$ in $H=20$ Oe can be seen in Fig. 4(j) at T_{IM} of the $x=0.16$ sample. The transitions at both T_{oo} and T_{IM} are from one magnetic phase to another, and the crystalline anisotropy can be expected to decrease in the two-phase transition region. A reduced crystalline anisotropy would give a stronger response of the magnetic system to a weak $H=20$ Oe applied field.

The $M(T)$ curves for $H=5$ kOe in Figs. 4(d)–4(f) show a sharp increase on cooling through the orbital order-disorder transition at T_{oo}; this increase is particularly marked at the first-order transition in the $x=0.11$ sample. The orbital ordering of the O'' phase clearly favors 3D ferromagnetic interactions in lower magnetic fields. Moreover, as x increases, the concentration and mobility of the ferromagnetically coupled Zener polarons increases near T_c, which strengthens the ferromagnetic double-exchange component of the magnetic interactions. Consequently, T_c increases and the transition at T_c becomes less glasslike; by $x=0.16$, a typical second-order anomaly in $C_p(T)$ is found at T_c. The $x=0.15$ sample is at the cross-over from vibronic to itinerant electronic behavior below T_c and at the convergence of $T_{\rm JT}$ and T_c. Consequently the entropy change at T_c suggests the coexistence of a vibronic and a metallic ferromagnetic phase.

Figure 4(k) shows two distinguishable Curie temperatures for the $x=0.17$ phase; they appear to represent the coexistence of the O^* and R phases and the discontinuity in T_c that occurs at the transition from the O^* to the R phase. The O^*-R transition at $T_{OR}<T_c$ within the phase of higher T_c is only weakly visible in the $C_p(T)$ trace; it is more clearly

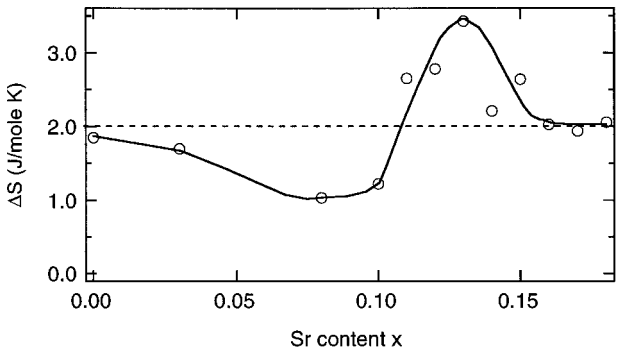

FIG. 5. Entropy change ΔS at T_N, T_c and T_{oo}, or T_c obtained from area of $C_p(T)/T$ after subtraction of background. Solid line is guide to the eye.

marked by a drop in $M(T)$ taken with $H=20$ Oe. The step in the $H=20$ Oe $M(T)$ curves, which show a thermal hysteresis in $M(T)$ for FC and ZFC in $H=20$ Oe as in the resistivity curves of Fig. 2, is clearly associated with a weakly first-order transition at $T_{\rm OR}<T_c$ in the $x=0.18$ and 0.19 samples in Figs. 4(l), 4(m). In Figs. 4(k)–4(m), the $C_p(T)$ anomalies at T_c are typical of second-order magnetic transitions. On the other hand, a small thermal hysteresis at T_c suggests some first-order character may accompany a transition from itinerant character below T_c to polaronic conduction above T_c (see Fig. 2). It is interesting that the ZFC and FC $M(T)$ curves for $H=20$ Oe in Fig. 4(k) for $x=0.17$ diverge below T_{IM}. This divergence is consistent with a glassy character of the spins in zero applied field in the O'' phase.

Figure 5 shows a plot of the entropy change ΔS obtained for T_N and T_c, T_{oo} after subtracting out the background (dashed line in Fig. 4) determined by fitting with polynomials. The value of ΔS obtained for T_N in the $x=0.00$ and 0.03 samples approaches the value of 2 J/mole K typically found[16] for a second-order transition in these perovskites, as does also ΔS at T_c for $0.16\leqslant x\leqslant 0.18$. However, ΔS is suppressed to half this value at $x=0.08$, which is indicative of a considerable volume of ferromagnetic short-range order far above T_N and of spins freezing without much change in the long-range order at T_N; the ferromagnetic volume is manifest in a larger $M(5\text{ K},50\text{ kOe})$ than expected for canted-spin ferromagnetism alone, Fig. 3. A contribution from the orbital order-disorder transition at $T_{oo}\leqslant T_g$ prevents observation of an even lower ΔS for the magnetic transition at T_g in the $x=0.10$ sample. The orbital order-disorder and disorder-order transitions at T_{oo} and T_c, respectively, make major contributions to ΔS in samples $0.12\leqslant x\leqslant 0.15$.

SUMMARY AND CONCLUSIONS

Measurements of resistivity $\rho(T)$, specific heat $C_p(T)$, magnetization $M(T)$ in applied magnetic fields $H=20$ Oe, 5 kOe and magnetization at 5 K up to 50 kOe have confirmed the complex phase diagram below 310 K of the system $La_{1-x}Sr_xMnO_3$ in the range $0.00\leqslant x\leqslant 0.35$ that has been deduced from magnetic and high-pressure transport data, structural experiments, and measurements made on individual samples by several groups. In the compositional range $0.08\leqslant x\leqslant 0.18$, the electrons in σ-bonding orbitals undergo a transition from localized behavior in a canted-spin antiferromagnetic insulator (CAFI) with a static, cooperative Jahn-Teller orbital ordering to itinerant-electron behavior in a ferromagnetic metal (FM). We have identified a spin-glass phase appearing in low applied magnetic fields between the CAFI and FM phases where the CMR phenomenon is found. The data allow a distinction to be made between growth in an applied field H of a FM minority phase in a paramagnetic matrix in the interval T_g (or T_c) $<T<T_{\rm JT}$ and the phase transformation from a spin-glass to a ferromagnetic vibronic (FV) phase on application of an $H=5$ kOe below $T_g\approx T_c$. The former is responsible for the CMR phenomenon; the latter represents stabilization in a magnetic field of an orbital disordering that is compatible with 3D ferromagnetic interactions relative to an orbital ordering that gives some antiferromagnetic interactions. As the Weiss molecular field of the ferromagnetic phase increases with T_c in the compositional range $0.10\leqslant x\leqslant 0.15$, the glassy character of the transition at $T_g\approx T_c$ decreases. Steps in T_c at the first-order vibronic-itinerant electronic transition at $x=0.15$ and the O^*-R transition at $x=0.17$ are manifest by evidence of the coexistence of two phases. Moreover, the transition from 3D to 2D orbital fluctuations confined to (001) planes on cooling through the transition at $T_{\rm JT}$ was shown to change from second-order to first-order as $T_{\rm JT}$ decreases to T_c at the transition from vibronic to itinerant electronic behavior at $x\approx 0.15$. The magnetization $M(5\text{ K},50\text{ kOe})$ is greater than the spin-only value $(4-x)\,\mu_B$/Mn in the FI phase below T_{oo}, reaching $4.4\,\mu_B$/Mn at $x=0.15$, but it has the spin-only value in the FM phase. An orbital moment adds to $M(T)$ where the e electrons are localized; itinerant electrons do not contribute an orbital component to the atomic magnetic moment.

The first-order T_{IM} transition in the narrow range $0.15\leqslant x\leqslant 0.17$ appears to be an extension of $T_{\rm JT}$, paramagnetism giving the orbital order of the O' phase below $T_{\rm JT}$ and ferromagnetism the orbital order of the O'' phase below T_{IM}. At the transition from localized to itinerant behavior of the electrons of e-orbital parentage, the system exhibits two intermediate configurations: one is a dynamic segregation of a FM phase within a CAFI matrix and the other is the retention of dispersed two-manganese Zener polarons that preferentially order their axes along an [001] axis in the O'' phase. Below T_{IM} the Zener polarons are more mobile than below T_{oo}. In the narrow temperature range $T_{oo}<T<T_g\approx T_c$, the orbital ordering in the matrix of the O' phase gives antiferromagnetic interactions along the [001] axis and, therefore, a spin glass. Dispersal of the Zener polarons favors 3D ferromagnetic interactions and a short-range orbital ordering that becomes progressively long-range ordered on cooling through T_{oo}. Condensation of holes into isolated FM clusters favors formation of a spin glass below $T_g\approx T_c$; application of a magnetic field stabilizes ferromagnetic order and therefore dispersal of the Zener polarons. As T_c increases and $T_{\rm JT}$ decreases with increased hole concentration x, condensation of the Zener polarons into FM clusters above T_c is reduced, so the glassy character of the transition at $T_g\approx T_c$ is

reduced. The polaronic-itinerant electronic transition at T_{IM} occurs below T_c, a polaronic-polaronic transition at T_{JT} occurs in the paramagnetic phase above T_c. This peculiar competition between orbital, charge, and magnetic order occurs in the compositional range between where T^* falls below T_N in Fig. 1 and T_{JT}, T_{IM}.

ACKNOWLEDGMENTS

The authors thank the Robert A. Welch Foundation and TCSUH, both of Houston, TX, and the NSF for financial support.

[1] J.-S. Zhou and J. B. Goodenough, Phys. Rev. B **60**, R15002 (1999).
[2] J. B. Goodenough, Phys. Rev. **100**, 564 (1955).
[3] E. F. Bertaut, in *Magnetism: A Treatise on Modern Theory and Materials*, edited by G. T. Rado and H. Suhl (Academic Press, New York, 1963), Chap. 4.
[4] J.-S. Zhou, J. B. Goodenough, Phys. Rev. B **62**, 3834 (2000); J.-S. Zhou, G.-L. Liu, J. B. Goodenough, *ibid.* **63**, 172416 (2001).
[5] B. Dabrowski, X. Xiong, Z. Bukowski, R. Dybzinski, P. W. Klamut, J. E. Siewenie, O. Chmaissem, J. Shaffer, C. W. Kimball, J. D. Jorgensen, and S. Short, Phys. Rev. B **60**, 7006 (1999).
[6] A. Urushibara, Y. Moritomo, T. Arima, A. Asamitsu, G. Kido, and Y. Tokura, Phys. Rev. B **51**, 14103 (1995).
[7] S. Jin, T. H. Tiefel, M. McCormack, R. A. Fastnacht, R. Ramesh, and L. H. Chen, Science **264**, 413 (1994).
[8] E. Dagotto, S. Yunoki, A. L. Malvezzi, A. Moreo, J. Hu, S. Capponi, D. Poilblanc, and N. Furukawa, Phys. Rev. B **58**, 6414 (1998); J. B. Goodenough, Aust. J. Phys. **52**, 155 (1999).
[9] M. J. Rozenberg, G. Kotliar, and X. Y. Zhang, Phys. Rev. B **49**, 10 181 (1994).
[10] Y. Moritomo, A. Asamitsu, and Y. Tokura, Phys. Rev. B **51**, 16491 (1995).
[11] G. R. Stewart, Rev. Sci. Instrum. **54**, 1 (1983).
[12] T. Okuda, A. Asamitsu, Y. Tomioka, T. Kimura, Y. Taguchi, and Y. Tokura, Phys. Rev. Lett. **81**, 3203 (1998).
[13] P.-G. de Gennes, Phys. Rev. **118**, 141 (1960).
[14] J. B. Goodenough, A. Wold, R. J. Arnott, and N. Menyuk, Phys. Rev. **124**, 373 (1961); J.-S. Zhou, H.-Q. Yin, and J. B. Goodenough, Phys. Rev. B **63**, 184423 (2001).
[15] S. Uhlenbruck, R. Teipen, R. Kingeler, B. Büchner, O. Friedt, M. Hücker, H. Kierspel, T. Niemöller, L. Pinsard, A. Revcolevschi, and R. Gross, Phys. Rev. Lett. **82**, 185 (1999).
[16] M. R. Lees, O. A. Petrenko, G. Balakrishnan, and D. Mck. Paul, Phys. Rev. B **59**, 1298 (1999).